Using three-dimensional discrete spherical Fourier descriptors based on surface curvature voxels for pollen particle recognition*

Xie Yong-Hua(谢永华)[a)b)†] and Michael OhEigeartaigh[b)]

[a)] *Institute of Computer Science, Nanjing University of Information Science and Technology, Nanjing* 210044, *China*
[b)] *School of Science, Waterford Institute of Technology, Waterford, Ireland*

(Received 20 January 2010; revised manuscript received 5 July 2010)

This paper presents a new method for extract three-dimensional (3D) discrete spherical Fourier descriptors based on surface curvature voxels for pollen particle recognition. In order to reduce the high amount of pollen information and noise disturbance, the geometric normalized curvature voxels with the principal curvedness are first extracted to represent the intrinsic pollen volumetric data. Then the curvature voxels are decomposed into radial and angular components with spherical harmonic transform in spherical coordinates. Finally the 3D discrete Fourier transform is applied to the decomposed curvature voxels to obtain the 3D spherical Fourier descriptors for pollen recognition. Experimental results show that the presented descriptors are invariant to different pollen particle geometric transformations, such as pose change and spatial rotation, and can obtain high recognition accuracy and speed simultaneously.

Keywords: curvature voxels, spherical coordinates, three-dimensional discrete Fourier descriptors, pollen particles recognition

PACC: 0650, 4230S

1. Introduction

Biological particle classification is one of the most important techniques in a wide range of applications, such as cell classification for auxiliary diagnosis, paleoclimatic reconstruction, derivation of geographical origin of products, study of allergenic processes in medicine, index forecasting for people with pollen hypersensitivity, etc.[1,2] The principal tasks in almost all of these applications are to classify and count biological particles, which should be done manually by highly skilled experts under the microscopy.[3] A high level of training is needed to obtain accurate identification results, and the commonly used discrimination criterion is the visual biological particle morphological appearance, such as shape, polarity, aperture, size, exine stratification and thickness, and so on.[4,5] This work is laborious and time consuming, and always brings about some wrong identifications. Pollen particle classification and recognition is of no exception which has been greatly focused on in recent years.[6,7] Due to the fact that different categories of pollen particles can be represented effectively through some intrinsic digitalised image features, such as morphology, texture, shape, geometric and statistical features, etc, using the technologies of computer vision and pattern recognition for automated pollen image classification has been an innovative approach to the cross-disciplinary research of computer vision, biology and environmental protection.[8,9]

Many useful algorithms have been developed to characterise the two-dimensional (2D) or three-dimensional (3D) pollen image features in recent years. Since most of the pollen images are usually recorded as a full 3D volumetric data set with confocal laser scanning microscopy, any 2D representation of these 3D pollen structures will involve a substantial loss of information. A clear tendency appears towards the study of cells and cell clusters including whole organisms in their natural 3D environment.[10] In recent years, some effective 3D pollen image features have been developed for characterising the 3D volumetric pollen particles recorded with a confocal laser scanning microscope, which include the following representative achievements. Reisert and Burkhardt[11] presented group integration invariant descriptors based

*Project supported by the National Natural Science Foundation of China (Grant No. 60472061), the Natural Science Foundation of Jiangsu Province, China (Grant No. BK20090149), and the Natural Science Foundation of Higher Education Institutions of Jiangsu Province, China (Grant No. 08KJD520019).

†Corresponding author. E-mail: yonghua@nuist.edu.cn

© 2010 Chinese Physical Society and IOP Publishing Ltd

on gradient operators and spherical harmonic expansion (GSGID) for 3D pollen classification, which achieved a 93.2% recognition rate. Ronneberger *et al.*[12] presented the MiSP invariants features in 3D volume space (MiSPID) for pollen classification, which obtained 96.0% general recognition rate. Fehr *et al.*[13] used voxel-wise gray invariants (VWGID) for 3D volumetric data classification and 94.6% recognition rate was obtained. Wang *et al.*[14] presented a continuous Fourier descriptors (CFD) in spherical coordinates and validated its excellent rotation and translation invariance for characterising the 3D objects, and the recognition rate by applying the experiment on the confoncal pollen database reached 92.7%. However most of the 3D pollen images usually display high dimensionality and redundant information caused by pollen pollution and noise disturbance. With all the above methods investigated directly are the features on the whole 3D pollen voxels, which can increase the computation cost greatly and make them inapplicable to practical pollen classification.[15,16]

In order to obtain high classification accuracy, the extracted discrimination features should be more compressed and invariant to the different pollen qualities. This paper takes both curvature voxels representation and 3D discrete Fourier transformation into consideration, and then presents the 3D discrete spherical Fourier descriptors (DSFD) based on surface curvature voxels for pollen particles recognition. Experimental results show that the presented descriptors are invariant to pollen image rotation, scale and translation, and can obtain high recognition accuracy and speed simultaneously.

The rest of this paper is organised as follows. In Section 2 the computation of geometric normalised surface curvature voxels is introduced. In Section 3, we present the process for extracting the DSFD based on curvature voxels decomposition in spherical coordinates. In Section 4 we present the classification algorithm and the comparative experimental results. Finally we draw some conclusions in Section 5 by summarizing our contribution and discussion topics for future work.

2. Geometrically normalised surface curvature voxels

Since the 3D pollen images usually have a huge amount of surface information as well as the noise caused by the sensors and the reconstruction process, it is desirable to have a more compact intermediate representation of 3D pollen images to reduce the redundant information and noise disturbance. Surface curvature has been used extensively in the literature for mesh simplification and smoothing, object recognition and mesh segmentation in 3D coordinates.[17,18] The corresponding curvedness measures the intensity of the surface curvature and describes how gently or strongly curved a surface is. The surface curvature voxels are actually the rigid feature points with the local curvature information at multiple scales, which can retain the principal structural information about surface curvedness and reduce the noise disturbance effectively. With a given threshold, the surface curvature voxels corresponding to the principal curvedness are selected as suitable kernel points for representing the intrinsic features of the pollen volumetric data. Mathematically, it can be defined as follows.

Let $z = f(x, y)$ be the function of the 3D image surface M in 3D rectangular coordinates. Let t_{p_i} be a tangent vector on the surface at the point $p_i \in M$ with $\|t_{p_i}\| = 1$, the normal curvature of M in the direction of t_{p_i} is defined as

$$\kappa(t_{p_i}) = S(t_{p_i}) \cdot t_{p_i}, \tag{1}$$

where $i \in [1, N]$, N is the total number of the pixel points on the surface M, $S(t_{p_i}) = -D_{t_{p_i}} U$ is the shape operator with U being the field of surface normal vectors defined in a neighbourhood of p, and $D_{t_{p_i}}$ the derivative of U with respect to t_{p_i}. To the normal curvature $\kappa(t_{p_i})$, the maximum and minimum principle curvatures, $\kappa_{\max}(p_i)$ and $\kappa_{\min}(p_i)$ respectively, can be obtained as the principal curvatures at the point $p_i \in M$, which can be defined as

$$\kappa_{\max}(p_i) = H(p_i) + \sqrt{(H^2(p_i) - K(p_i))}, \tag{2}$$

$$\kappa_{\min}(p_i) = H(p_i) - \sqrt{(H^2(p_i) - K(p_i))}, \tag{3}$$

where $H(p_i)$ and $K(p_i)$ denote the mean curvature and the Gaussian curvature at the point $p_i \in M$ respectively.

Then the bending energy of the surface named curvedness at the point $p_i \in M$ is obtained as

$$C(p_i) = \sqrt{(\kappa^2_{\max}(p_i) + \kappa^2_{\min}(p_i))/2}. \tag{4}$$

The curvedness can be used to indicate how strongly or gently curved a surface is. When the curvedness at a given point approaches zero, the surface patch around this point will become planar gradually. The curvedness will be zero for those completely planar

surface patches. Therefore, the higher curvedness actually reflects the sharp bending degree of surface patch, which can effectively describe the primary local surface features. In order to reduce a large amount of redundant information, a threshold is used to select the surface points with the principal curvedness as the curvature voxels, which can be described as follows.

Let $\{p_1, p_2, \ldots, p_i, \ldots, p_N | p_i(x_i, y_i, z_i) \in R^3\}$ be the collection of all the points on the 3D volumetric image surface M, then the mean of the curvedness for all the points will be computed as

$$\overline{C} = \frac{1}{N} \sum_{i=1}^{N} C_{p_i}. \tag{5}$$

Taking the curvedness mean as the threshold, the curvature voxels collection P with the principal curvedness can be selected as the feature points and given as

$$P = \{p_j | C_{p_j} \geq \overline{C}; j \in [1, N']\}, \tag{6}$$

where N' is the number of the selected curvature voxels in the collection P.

In the segmentation step of pollen classification, most of the pollen images are segmented and captured directly from the slides with different geometric poses. The geometry normalisation step is needed to insure the geometric invariance for most of the 3D images. The goal is to reorient the curvature voxels through a geometric affine map in 3D space, which will make the voxels invariant to the pollen geometric transformation of translation, rotation and scaling. Let A be the area of the 3D object surface M, which can be computed from the equation

$$A = \int\int_M \sqrt{1 + \left(\frac{\partial z}{\partial x}\right)^2 + \left(\frac{\partial z}{\partial y}\right)^2}\, \mathrm{d}x\mathrm{d}y,$$

the centre of gravity of the 3D model is expressed as

$$c = A^{-1} \int\int_M p_j \mathrm{d}s. \tag{7}$$

Based on the normalised centre of gravity, the translation invariance on the original curvature voxels is obtained as

$$P_c = \{p_j^c | p_j^c = p_j - c\}. \tag{8}$$

Taking the centre of gravity c as the origin, the canonical coordinates can be created to describe the 3D object in a uniform frame. Then with the following affine maps of rotation and scaling:

$$\varphi(P_c) = s^{-1} \cdot R \cdot p_j^c, \tag{9}$$

the final geometrically normalised curvature voxels are obtained, which can be described as

$$P' = \{p'_j | j \in [1, N']\}, \tag{10}$$

where s and R are the scaling operator and the rotation operator defined in Ref. [19].

The transformed image $M(p'_j)$ based on the discrete curvature voxels can be used to represent the principal 3D image surface information, which can greatly reduce the redundant information and noise disturbance on the surface. The extracted features based on the curvature voxels will be more compact and robust than those directly extracted from the original 3D images.

3. 3D discrete Fourier descriptors

3.1. Curvature voxels decomposition in spherical coordinates

After characterising 3D images with curvature voxels, the next step is to define a robust feature vector based on curvature voxels. For 3D images that are usually taken to be of a certain rotational symmetry, it is more effective to represent the 3D image on a sphere in a rotation invariant manner. Since 3D images can be decomposed into wave-like basic patterns that have simple radial and angular structures, we utilize the spherical harmonics[20,21] to decompose the curvature voxel-based image function in 3D spherical coordinates, which can be described as the following steps.

The curvature voxels in the canonical rectangular coordinates should first be represented in polar form in 3D spherical coordinates. For each curvature voxel p'_j, the feature value $M(p'_j)$ can be mapped into a spherical field $S(\boldsymbol{n})$, where $\boldsymbol{n} = (\sin\phi\cos\theta, \sin\phi\sin\theta, \cos\phi)$ is a vector denoting the voxel position on the sphere surface. There is a one-to-one relationship between the curvature voxel $S(\boldsymbol{n})$ on the sphere and p'_j of the original 3D object. In relation to the solution of the Helmholtz equation, the basis function $S(\boldsymbol{n})$ will be decomposed into radial and angular components, which take the separation form as

$$S(\boldsymbol{n}) = R(r)\, \Phi(\theta, \phi), \tag{11}$$

where (r, θ, ϕ) are the spherical coordinates, $R(r)$ is the radial component which can be defined by the

spherical Bessel function of order l and is related to the ordinary Bessel Function J_l by

$$R_{k,l}(r) = S\mathrm{J}_l(kr) = \sqrt{\frac{\pi}{2kr}}\mathrm{J}_{l+1/2}(kr). \quad (12)$$

Due to the fact that the 3D image surface is described by the discrete curvature voxels, the parameter k can take discrete values, which means that the discrete image function is defined on a finite interval with zero-value boundary condition. The angular part $\Phi(\theta,\phi)$ of the basis function actually is a spherical harmonics defined on a unit sphere, which can be obtained by the spherical harmonic transformation

$$\Phi(\theta,\phi) = Y_l^m(\theta,\phi) = C_l^m P_l^m(\cos\theta)\mathrm{e}^{\mathrm{i}\,m\phi}, \quad (13)$$

where C_l^m is a constant, P_l^m is an associated Legendre polynomial, order l is a positive integer or zero, repetition m is a non-zero integer subject to the following constraints: $l-|m|$ is even and $|m| \le l$.

The angular part of the basic function is represented by spherical harmonic features, which can be calculated on the spherical surfaces of different radii and collected to describe the rotation-invariant features of a 3D object.

Combing the radial part and the angular part together, the normalised basis function for spherical Fourier transform is defined on an image spherical surface

$$\psi_{k,l}^m(r,\theta,\phi) = \sqrt{\frac{2}{\pi}}k\mathrm{J}_l(kr)Y_l^m(\theta,\phi). \quad (14)$$

The combined separation form treats each spherical surface as being independent of each other and has a good localisation nature. It describes the relation of angular properties of different radii as a whole, therefore can represent the radial structures effectively. Furthermore, the separation form of the basis function provides computational convenience and is more applicable to being transformed into the frequency coefficients by the transform methods, which can be directly used to compute the invariant discriminative descriptors.

3.2. 3D discrete Fourier descriptors

Based on the decomposition of the geometry-normalised curvature voxels into separated radial and angular forms in spherical coordinates, we will continue to use a transformation method to extract frequency coefficients and the corresponding descriptors. The spherical Fourier transform is a commonly used frequency transformation method in 3D spherical coordinates, whose advantage is that when a 3D image is rotated around the origin, the variations of its transformed coefficients can be relatively simply expressed in terms of the rotation parameters. This performance can be used to estimate rotation parameters and extract invariant descriptors simultaneously.

For the discrete 3D image function S at the new location $\boldsymbol{n}$, it can be expanded using the normalised basis function $\psi_{k,l}^m$

$$S(\boldsymbol{n}) = \sum_{k=1}^{k_0}\sum_{l=0}^{L}\sum_{m=-l}^{l} V_{k,l}^m\psi_{k,l}^m, \quad (15)$$

where the spherical Fourier coefficients $V_{k,l}^m$ are the inner product of the field $S(\boldsymbol{n})$ and the spherical basis function, which can be described as the discrete form

$$V = \sum_{i=1}^{N'} S(\boldsymbol{n}_i)\omega(\boldsymbol{n}_i)^{\mathrm{H}}(W^{\mathrm{H}}W)^{-1}, \quad (16)$$

where $\omega(\boldsymbol{n}_i) = [\psi_{k,0}^0(\boldsymbol{n}), \psi_{k,1}^{-1}(\boldsymbol{n}), \psi_{k,1}^0(\boldsymbol{n}), \ldots, \psi_{k,L}^L(\boldsymbol{n})]$, $W = [\omega(\boldsymbol{n}_1), \ldots, \omega(\boldsymbol{n}_{N'})]^{\mathrm{T}}$, H denotes the Hermitian transpose, k_0 is a certain discrete parameter and satisfies $k_0 > 1$.

When the discrete pollen image $S(\boldsymbol{n})$ with the discrete spherical Fourier coefficient $V_{k,l}^m$ is under the rotation $R(\alpha,\beta,\gamma)$, the transform can be described as

$$R(\alpha,\beta,\gamma)S(\boldsymbol{n}) = R(\alpha,\beta,\gamma)\sum_{k=1}^{k_0}\sum_{l=0}^{L}\sum_{m=-l}^{l} V_{k,l}^m\psi_{k,l}^m. \quad (17)$$

Due to the fact that all the variance of the basis function $\psi_{k,l}^m$ under rotation is described by the angular part, the rotation operator $R(\alpha,\beta,\gamma)$ can be applied to $\psi_{k,l}^m$ directly with the Wigner-D function $D_{mm'}^{(l)}$.[12] The equation can be written as

$$\begin{aligned} R(\alpha,\beta,\gamma)S(\boldsymbol{n}) &= \textstyle\sum_{k=1}^{k_0}\sum_{l=0}^{L}\sum_{m=-l}^{l} V_{k,l}^m \sum_{m'=-l}^{l} D_{mm'}^{(l)}(\alpha,\beta,\gamma)\psi_{k,l}^{m'} \\ &= \textstyle\sum_{k=1}^{k_0}\sum_{l=0}^{L}\sum_{m=-l}^{l}[\sum_{m'=-l}^{l} D_{mm'}^{(l)}(\alpha,\beta,\gamma)V_{k,l}^{m'}]\psi_{k,l}^m, \end{aligned} \quad (18)$$

where $D_{mm'}^{(l)}(\alpha,\beta,\gamma)$ with m and $m' = -l, -l+1, \ldots, l$ forms a $(2l+1)\times(2l+1)$ matrix called the Wigner-D matrix.[12] The rotation parameter $R(\alpha,\beta,\gamma)$ can be directly coded into the change of the spherical Fourier coefficients

$$V_{k,l}^{m} \Rightarrow \sum_{m'=-l}^{l} D_{mm'}^{(l)}(\alpha,\beta,\gamma)V_{k,l}^{m'}. \quad (19)$$

As the Winger-D matrix is unitary, it is obvious that rotating a spherical function will not change its L_2-norm, namely the magnitude of the spherical Fourier coefficient $V_{k,l}^{m}$ remains unchanged. Therefore we can represent the energies of coefficients as the rotation-invariant property of the 3D object

$$\|V_{k,l}^{m}\| = \sqrt{\sum_{m=-l}^{l} |V_{k,l}^{m}|^2} = \sqrt{\sum_{m=-l}^{l} V_{k,l}^{m}(V_{k,l}^{m})^*}. \quad (20)$$

The magnitude $\|V_{k,l}^{m}\|$ is the corresponding DSFD, which can be used as the geometric invariant features for 3D image recognition and classification. First, the curvature voxels reflecting the curvedness and direction of the 3D image surface cannot only reduce the high dimensionality, but also control or relieve the noise disturbance to the pixel values. Furthermore, the curvature voxels of any the same category pollen images are different from those of the other categories, which can receive good performance of distinguishability. Second, the proposed 3D discrete Fourier descriptors in spherical coordinates based on geometrically normalised curvature voxels are robust to image rotation, translation and scaling transformation.

4. Experimental results

Experiments are performed on two pollen image datasets with a Pentium IV computer of 2.8 GHz CPU and 2 GB memory. Dataset 1 is the laboratory confocal pollen image dataset with 389 pollen particles of 26 different taxa, in which the images were directly from the corresponding plants and are manually recorded as a full 3D volumetric data set with confocal laser scanning microscopy. Dataset 2 is the real-world pollenmonitor dataset with 22750 pollen particles from 33 taxa, in which the images were automatically collected, prepared and recorded by the first prototype of the pollenmonitor in Europe in 2006.[22] All the images in the both datasets take on different appearances, such as pose change, spatial rotation, and so on. In order to validate the good geometric invariant performance of our proposed DSFD descriptors, all the images were not be geometrically normalised before the feature extraction. The final test was performed by taking 20% of the images of each category as training images and the remaining ones as test images with random selection. The support vector machine classifier with kernel function $k(x,y) = exp(-\gamma\|x-y\|)^2/2$ is used for the final feature classification. The measurements of features number (FN), correct recognition rate (CRR), rejected rate (RR), false recognition rate (FRR) and recognition time (RT) are used to evaluate the recognition performance of the descriptors.

Figure 1 presents the partially classified results for the two categories of pollen images of Alnus (Erle) and Betula (Birke). It can be seen that most of the pollen images with different pose changes and spatial rotations can be correctly recognized. The detailed results are as follows.

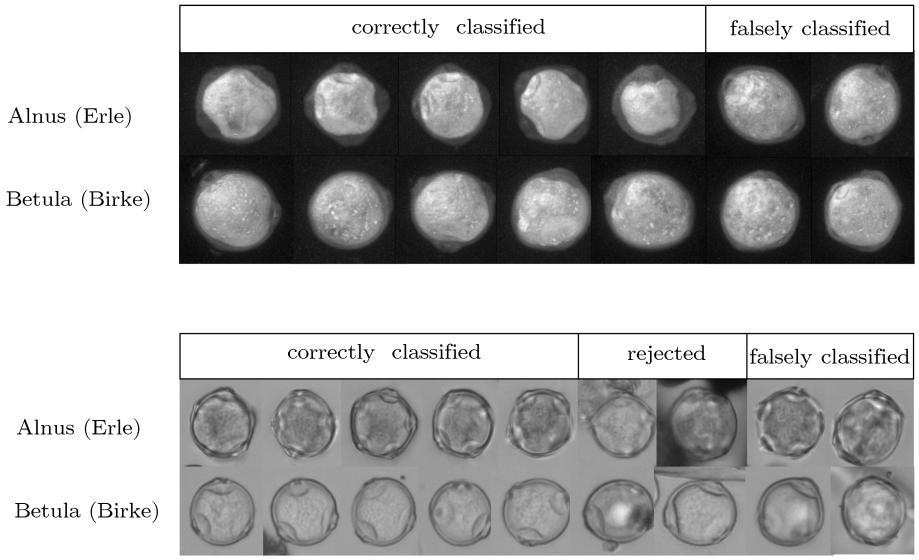


Fig. 1. Partial correctly, rejected and falsely classified examples. (a) Examples on pollen image Dataset 1, (b) examples on pollen image dataset 2.

For the confocal pollen images in dataset 1, all the pollen images in these two categories can be correctly classified without any rejected image. For the pollenmonitor images in dataset 2, most of the pollen images can be correctly classified, and the rejected rate and false recognition rate on Alnus (Erle) and Betula (Birke) pollens can be kept at 8.8% and 6.4% respectively. The false recognized samples are caused mainly by the slight shape and pose changes of 3D pollen images. Furthermore, the illumination change and the pollen pollution will make the curvature voxels and the extracted descriptors changed at the same time, which will cause some pollen images to be rejected. The recognition results on 5 classic pollen taxa in two datasets are presented in Table 1. It can be seen that the recognition performance varies with pollen taxa because of the variance in pollen image quality. However, satisfactory recognition results can still be obtained on different categories of pollen images, especially for those images with high qualities and clear structures, such as Alnus and Betula pollen particles.

Table 1. Recognition results on 5 classic pollen taxa in two datasets.

image dataset	pollen taxa	CRR/%	RR/%	FRR/%
dataset 1	Alnus (Erle)	97.2	0	2.8
	Betula (Birke)	98.6	0	1.4
	Corylus (Hasel)	91.7	3.2	5.1
	Fraxinus (Esche)	92.3	2.8	4.9
	Quercus (Eiche)	90.1	4.6	5.3
dataset 2	Alnus (Erle)	91.2	3.7	5.1
	Betula (Birke)	93.6	3.8	2.6
	Corylus (Hasel)	86.4	7.6	6.0
	Fraxinus (Esche)	89.8	5.8	4.4
	Quercus (Eiche)	87.2	8.2	4.6

Furthermore, in order to test the efficiency of our proposed features, we compare the average recognition performance of our DSFD method with that of the four recently developed methods, which include the GSGID method,[11] the MiSPID method,[12] the VWGID method[13] and the CSFD method,[14] on the two pollen image datasets. Table 2 gives the comparison among average recognition results obtained from different methods. It is obvious that our DSFD method can obtain better recognition performance than the other four methods. First, the DSFD method can obtain a similar high correct recognition rate to that of the MiSPID method, which also outperforms that of the other three methods by 4.5% averagely. Second, the DSFD features are extracted based on the discrete surface curvature voxels, which can greatly compress the redundant information and reduce the high dimensionality of the 3D pollen image. For example, compared with the CSFD, the DSFD can reduce the feature number by about 90% and the recognition time for 389 images in dataset 1 and 22750 images in dataset 2 can be calculated to be 2.2 s and 4.9 s respectively. The contrast results further validate that our proposed DSFD descriptors are not only invariant to different pollen geometric transformations, such as pose change and spatial rotation, but also quite suitable for practical pollen classification and recognition.

Table 2. Comparison average recognition results with different features.

descriptors	image dataset	FN	CRR/%	RR/%	FRR/%	RT/s
GSGID	dataset 1	7680	93.2	4.6	2.2	15.3
	dataset 2	26820	83.3	13.2	3.5	20.9
MiSPID	dataset 1	8960	96.0	1.4	2.6	16.2
	dataset 2	87296	92.0	5.2	2.8	28.3
VWGID	dataset 1	3500	94.6	2.3	3.1	8.5
	dataset 2	13620	85.0	9.5	5.5	13.7
CSFD	dataset 1	3375	92.7	2.7	4.6	8.2
	dataset 2	4500	86.5	8.3	5.2	12.6
DSFD	dataset 1	268	96.3	1.2	2.5	2.2
	dataset 2	729	91.8	4.9	3.3	4.9

5. Conclusion

This paper presents a new method to extract 3D DSFD based on surface curvature voxels for pollen recognition. The advantages of our method are indicated in two aspects. First, the discrete curvature voxels can be used to represent the principal 3D pollen image surface information, which can greatly reduce the redundant information and noise disturbance on the 3D pollen image surface. Second, the extracted DSFD features are invariant to different pollen image geometric transformations, such as pose change and spatial rotation. The effective feature description ability and geometric invariance make our methods quite suitable for practical pollen recognition. Our future work will focus on the invariant descriptors based on local curvature voxels for quality-reduced 3D pollen images.

References

[1] Bush M B and Weng C Y 2007 *J. Biogeography* **34** 377

[2] Wang W, Bao L F, Liu H J, Yue X, Chen J H, Li H, Ren L H, Tang D G, Shiro H and Akinori T 2007 *Chin. Phys.* **16** 2818

[3] Chang S J, Chen Y, Guo P, Jia L P, Wang X H and Zhang T N 2010 *Acta Phys. Sin.* **59** 271 (in Chinese)

[4] Zhou X L, Chen X R, Yang X D and Gou Q Q 2003 *Chin. Phys.* **12** 1011

[5] Liao C, Liu D G and Liu S G 2009 *Acta Phys. Sin.* **58** 6709 (in Chinese)

[6] Li Z, Zhang J S, Yang J and Gong Q H 2006 *Chin. Phys.* **15** 2558

[7] Oliver E, Enrico M, Carsten Z and Hans A K 2001 *Chin. Phys.* **10** 100

[8] Alian B, Pablo J H, Monique T, Jordina B, Carmen G, Pierre B and Regis T 2002 *Aerobiologia* **8** 195

[9] Chang S J, Li X G, Shen J Y and Zhang Y X 2005 *Acta Phys. Sin.* **54** 5157 (in Chinese)

[10] Pierre B, Alian B, Monique T, Regis T, Pablo G H, Jordina B and Carman G 2002 *Image Anal. Stereol.* **20** 527

[11] Reisert M and Burkhardt H 2006 *Proceedings of the 18th International Conference on Pattern Recognition*, HongKong, August 20–24, 2006 p206

[12] Ronneberger O, Burkhardt H and Schultz E 2002 *Proceedings of 16th conference on Pattern Recognition*, Canada, August 11–15, 2002 p290

[13] Fehr J, Ronneberger O, Haymo K and Burkhardt H 2005 *Proceedings of the 27th DAGM Symposium on Pattern Recognition*, Austria, August 30–September 2, 2005 p377

[14] Wang Q, Ronneberger O and Burkhardt H 2009 *IEEE Transactions on Pattern Analysis and Machine Intelligence* **31** 1715

[15] Ranzato M, Taylor P E, House J M, Flagan R C, LeCun Y and Perona P 2007 *Pattern Recognition Letters* **28** 31

[16] Alain B and Thonnat M 2002 *Proceedings of the 18th International Conference on Pattern Recognition*, Hong Kong, August 20–24, 2006 p800

[17] Huy T H and Danny G 2008 *Proceedings of the 2008 Digital Image Computing: Techniques and Applications*, Australia, December 1–3, 2008 p16

[18] Rieger B, Timmermans F J, Van Vliet L J and Verbeek P W 2004 *IEEE Transactions on Pattern Analysis and Machine Intelligence* **26** 1088

[19] Vranic D V and Saupe D 2001 *Proceedings of the EURASIP Conference on Digital Signal Processing for Multimedia Communications and Services*, Hungary, September 11–13 2001 p271

[20] Micheal K, Thomas F and Szymon R 2003 *Proceedings of the 2003 Eurographics/ACM SIGGRAPH symposium on geometry processing*, Germany, June 23–25 2003 156

[21] Ren H P, Ping Z L, Bo W L G, Sheng Y L, Cheng S Z and Wu W K 2003 *Chin. Phys.* **12** 610

[22] Ronneberger O 2007 *3D Invariants for Automated Pollen Recognition* Ph.D. Thesis, Germany: Freiburg University